J Appl Electrochem (2017) 47:467–477
DOI 10.1007/s10800-017-1056-3

RESEARCH ARTICLE

The influence of an aqueous-butanol plating bath on the microstructure and corrosion resistance of electrodeposited nickel coatings

Ryan E. Daugherty[1] · Madeline M. Zumbach[1] · Teresa D. Golden[1]

Received: 8 November 2016 / Accepted: 6 February 2017 / Published online: 23 February 2017
© Springer Science+Business Media Dordrecht 2017

Abstract The effects of higher concentrations (5 and 10%) of an organic modifier, butanol, added to an aqueous electroplating solution for nickel deposition have been studied. Nickel coatings were deposited on steel substrates from a modified all-sulfate bath with 5 and 10% additions of butanol under acidic conditions, while a modified pulse potential was applied. X-ray diffraction of the resulting nickel coatings showed a preferred (220) orientation for the crystal structure. The coatings were nanocrystalline with particle sizes between 16 and 35 nm as calculated from Williamson–Hall analysis. No cracking of the films was observed in the scanning electron microscopy images, even as the percentage of butanol increased, as typically is observed in other aqueous-organic baths. Corrosion resistance of the nickel coatings in a 3.5% sodium chloride solution was best for coatings deposited from plating solutions containing 5 and 10% butanol. E_{corr} was shifted from −0.405 V for the nickel coating from the additive-free bath to −0.234 V for the nickel coating from the 5% butanol solution. EIS results indicated a twofold improvement in charge transfer resistance for nickel coatings deposited when butanol was used in the plating bath. The advantages of using higher percentages of organic modifiers like butanol to enable the use of non-electroactive particles for production of composite coatings are discussed.

Electronic supplementary material The online version of this article (doi:10.1007/s10800-017-1056-3) contains supplementary material, which is available to authorized users.

✉ Teresa D. Golden
tgolden@unt.edu

Ryan E. Daugherty
rdaugherty432@gmail.com

[1] Department of Chemistry, 1155 Union Circle #305070, University of North Texas, Denton, TX 76203, USA

Graphical abstract

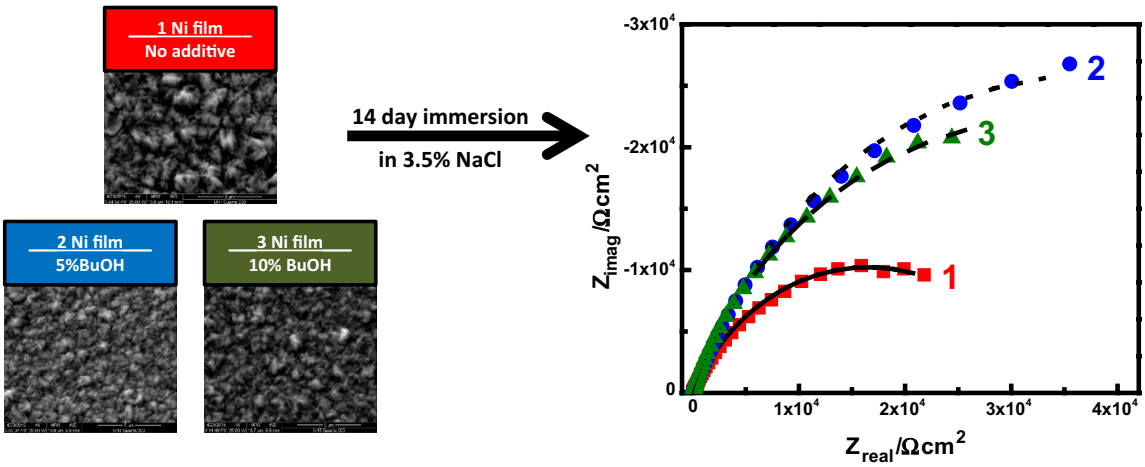

Keywords Nickel · Butanol · Electrodeposition · Corrosion · Nanocrystalline Coatings

1 Introduction

Corrosion inhibitive coatings are effective at preventing undesirable corrosion of many materials [1–5]. Nickel coatings are widely used to create protective coatings for marine engineering, aeronautical, and other general decorative applications [6, 7]. Nickel coatings are valued for providing strong adhesion to stainless steels, good mechanical properties, and corrosion resistance for the underlying steel [8–12]. Nanocrystalline nickel coatings, which have increased resistance to pitting corrosion, can be produced using electrodeposition [10, 13]. In recent years, additional components (i.e., ceramics, metal oxides, polymers) have been added to nickel coatings to improve the protection mechanism of the coatings in corrosive environments. These composite metal coatings have been studied for their improved physical and corrosion-resistant properties [14]. Additional components chosen for inclusion into coatings are often limited by their water solubility or flocculation properties in electrochemical baths [15]. Thus, synthetic routes such as casting, accumulative roll bonding, and hot dip methods are often used, but at higher costs and often with loss of control over morphology [16, 17].

Recently, a number of new electrolyte systems have been developed to lower the cost and widen the pH range for nickel deposition; however, the most common still in use are Watts type baths, which take advantage of the complexing effects of borate ions and their ability to cathodically shift hydrogen evolution [18–22]. Boric acid has a long history as an additive for nickel electrodeposition and has been shown to provide a buffering effect at the electrode surface, decreasing the amount of hydrogen embrittlement in Ni coatings [23, 24]. Though the mechanism is not well understood, boric acid forms a weak complex with nickel in solution that is advantageous for deposition at low current densities, which is necessary for nanocrystalline nickel deposition [21, 25, 26].

Addition of organic solvents can also improve the mechanisms of crystal growth and morphology, but the resultant corrosion inhibition of these nickel coatings has not been tested [27–31]. Some instances of aqueous-organic systems used to deposit metal coatings have been reported [32–34]. Previously, *N, N*-dimethylformamide (DMF) was a successful organic modifier to control microstructure, current efficiency, and hardness for nickel electrodeposits [28, 34]. More recently, nickel-based alloys and nanocomposite coatings electrodeposited in pure DMF were examined as aprotic solvent baths to deposit metals that typically cannot undergo deposition in aqueous systems [35, 36]. Microcracking is often observed in these systems due to internal strain from the growth mechanism caused by large amounts of DMF.

Aliphatic alcohols have also been used as modifiers to generate fine-grained nickel electrodeposits [27, 37–39]. The addition of unsaturated alcohols such as 2-butyne-1,4-diol and propargylic alcohol into a nickel electroplating bath was shown by Macheras et al. to induce inhibited growth modes on nickel crystallization during electrodeposition but did not control isolated or polycrystalline growth planes [37]. Nakamura et al. studied the effects of *n*-propyl, allylic, and propargylic alcohol and reported that these aliphatic alcohols caused a cathodic shift in the reduction potential of nickel as well as an inhibitory effect on the current efficiency in Watts' type baths [38]. As unsaturation of the molecule increased, the reduction potential shifted more cathodically. Costavaras reported that both cis and trans 2-butene-1,4-diol completely inhibited the

discharge of nickel above a concentration of 25 mM [27]. Oxygen-containing species, like these diols, containing unsaturated bonds will adsorb parallel to the electrode surface and be hydrogenated, which is beneficial; but potentially this decreases the natural efficiency of the boric acid species to remove adsorbed hydrogen at the electrode surface [39]. This adsorption affinity also limits the amount of additive that can be added into the plating solution. Even though increasing unsaturation helps dehydrogenate the electrode surface, the alcohol will strongly adsorb and can shut down the reaction if the concentration is too high. Typically, no more than 50 mmol (~0.05%) of alcohol additive can be added to the plating solution.

Electrodeposition of composite materials for use as corrosion inhibitive coatings containing nanoparticle size dopants is a growing field of research, but thus far is limited to purely aqueous systems. Therefore, development of organic-aqueous bath systems that allow both deposition of nickel coatings and stabilization of any non-soluble dopants for these coatings is of great interest [40]. Our literature survey uncovered no information on *n*-butanol (BuOH) as a modifier for nickel electrodeposition. BuOH has terminal alcohols and no unsaturated bonds, with a non-polar chain that can act as a pseudo-surfactant, potentially stabilizing non-hydrophilic nanoparticles. Additionally, borate ions are important in complexing with nickel and facilitating the reduction process that can be inhibited by diol compounds, which are known to complex with borate species in solution [41, 42]. Therefore, exploring new organic additives for plating solutions that can produce a wide variety of composite coatings at low temperatures, with small grain size and low strain, is in order. These aqueous-organic bath systems can help stabilize nanoparticles of very low solubility during electrodeposition of metal–matrix nanocomposite coatings. Others have developed modified bath systems which help stabilize colloids in aqueous and non-aqueous media [43, 44].

The present work establishes a method to deposit smooth, semi-bright nickel coatings, from a novel nickel bath at room temperature, with much larger concentrations (5 and 10%) of butanol, as an organic modifier, than has been used in previous diol studies. The morphology of these deposits is studied to determine the effect BuOH has on the reduction potential, growth inhibition, strain, and corrosion resistance to chloride attack for a series of nickel coatings deposited from baths containing 5 and 10% BuOH. Higher percentages of organic modifiers in the aqueous plating bath would help open up the use of non-electroactive components to produce new composite coatings.

2 Experimental

2.1 Materials

All reagents were of analytical grade and used as-received with no further processing. Nickel coatings were electrodeposited from solutions containing 26.29 g L^{-1} $NiSO_4.6H_2O$ (Alpha Aesar), 57.21 g L^{-1} $Na_2B_4O_7{\cdot}10H_2O$ (Fisher), and butanol (Mallinckrodt), adjusted to pH 3.0 ± 0.05 using 5 M H_2SO_4 (EM Scientific). By using sodium tetraborate and adjusting the pH with sulfuric acid, sodium borate is converted to boric acid leaving an excess of sodium and sulfate ions [42]. Sodium cations can initially increase conductivity of the solution and also maintain higher conductivity throughout deposition, as Ni is deposited from solution. The solvent composition of the plating baths was designated as A1 (no BuOH addition), B1 (5% of BuOH added), and B2 (10% BuOH added).

2.2 Electrodeposition of nickel coatings

An EG&G PAR potentiostat/galvanostat model 273 A was used for all depositions. Nitrogen was bubbled in all solutions prior to and during electrodeposition. The electrode substrates were 15 mm stainless steel 430 disks (Ted Pella), attached to copper leads with conducting silver-based epoxy and coated in resin epoxy to expose only one face. The composition of substrates is as follows: Fe, with 16.0–18.0% Cr, and less than 1.0% of Ni, C, Mn, P, S, and Si. 430 stainless steel working electrodes were prepared by polishing with 320 to 1200 grit SiC pads, followed by a final polish with 0.30 μm alumina. Electrodes were submerged in 5 M H_2SO_4 for 120 s, rinsed with DI H_2O, and dried just prior to deposition and cyclic voltammetry studies. Electrodeposition for all nickel coatings was carried out using a modified pulse potential consisting of −1.08 V for 10 s followed by −0.6 V for 4 s, scanning at 100 mV s^{-1} between steps, until a total charge of ~40.0 coulombs was reached [26, 45]. The resulting coatings were ~6 μm thick for all experimental runs.

2.3 Characterization techniques

A Thermo Orion 550 A conductivity meter with a Thermo Orion 013005 A platinum black four-cell conductivity probe was used to measure conductivity of the plating baths. Cyclic voltammetry (CV), open circuit potential immersion testing (OCP), Tafel polarization, and electrochemical impedance spectroscopy (EIS) studies were performed with a PAR Parstat 4000 potentiostat (Ametek). Cyclic voltammetry for the solutions was carried out in a three-electrode cell system that is composed of a stainless steel (SS) working electrode, chromel counter electrode,

and a saturated calomel (SCE) reference electrode. Potentiodynamic polarization, EIS, and OCP were all performed in a solution of 3.5% sodium chloride diluted with deionized water. The EIS was scanned from 10^5 Hz to 25 mHz with a perturbation amplitude of 10 mV. Potentiodynamic polarization scans were run from ±250 mV at a scan rate of 1 mV s^{-1}. Coating morphology was characterized by an Environmental FEI Quanta 200 scanning electron microscope at a magnification of ×25,000. Powder X-ray diffraction measured crystallinity and composition of the coatings with a Siemens D-500 X-ray diffractometer. Scans were run from 30–100 degrees 2θ at a 1 s dwell time and 0.05° step size, using CuK_α radiation with the tube set to 35 kV and 24 mA. Coating thickness was measured with a Veeco Dektak 8 stylus profilometer.

3 Results and discussion

3.1 Reduction potential of nickel and the effect of BuOH

Cyclic voltammetry was run for each of the plating bath systems (pH 3 ± 0.05) to determine the effects of BuOH on the nickel reduction potential. Each solution was scanned starting from OCP, between 0.5 V and −2.0 V, at a scan rate of 10 mV s^{-1}. The reduction and oxidation potentials of each bath are presented in Table 1. Cyclic voltammograms for each sample bath (Fig. 1) are displayed with and without the presence of nickel. Electrolyte bath systems containing no nickel are shown with α designations and were performed to subtract any capacitive effects of BuOH on the scan. The addition of BuOH in B1 (5%) and B2 (10%) shifted the reduction potential of nickel to slightly more cathodic potentials, around −1.25 V. This is consistent with Nakamura's findings that aliphatic alcohols do cause a cathodic shift in the reduction potential of nickel [38]. The current slightly decreased as BuOH percentage increased, due to a larger amount of adsorption onto the electrode surface, limiting the active area for nucleation. Hydrogen evolution in the cathodic region is typically observed at overpotentials beyond −1 V; however, boric acid species in solution shift the reduction of water to potentials that lie cathodic to that of nickel reduction [26].

Table 1 E_{pc}, E_{pa}, i_{pc}, and i_{pa} for each sample measured from cyclic voltammetry at a scan rate of 10 mV s^{-1}

Sample	E_{pc} (V)	i_{pc} (mA)	E_{pa} (V)	i_{pa} (mA)
A1	−1.22	18.4	−0.300	0.484
B1	−1.33	15.0	−0.300	0.465
B2	−1.27	14.7	−0.287	0.853

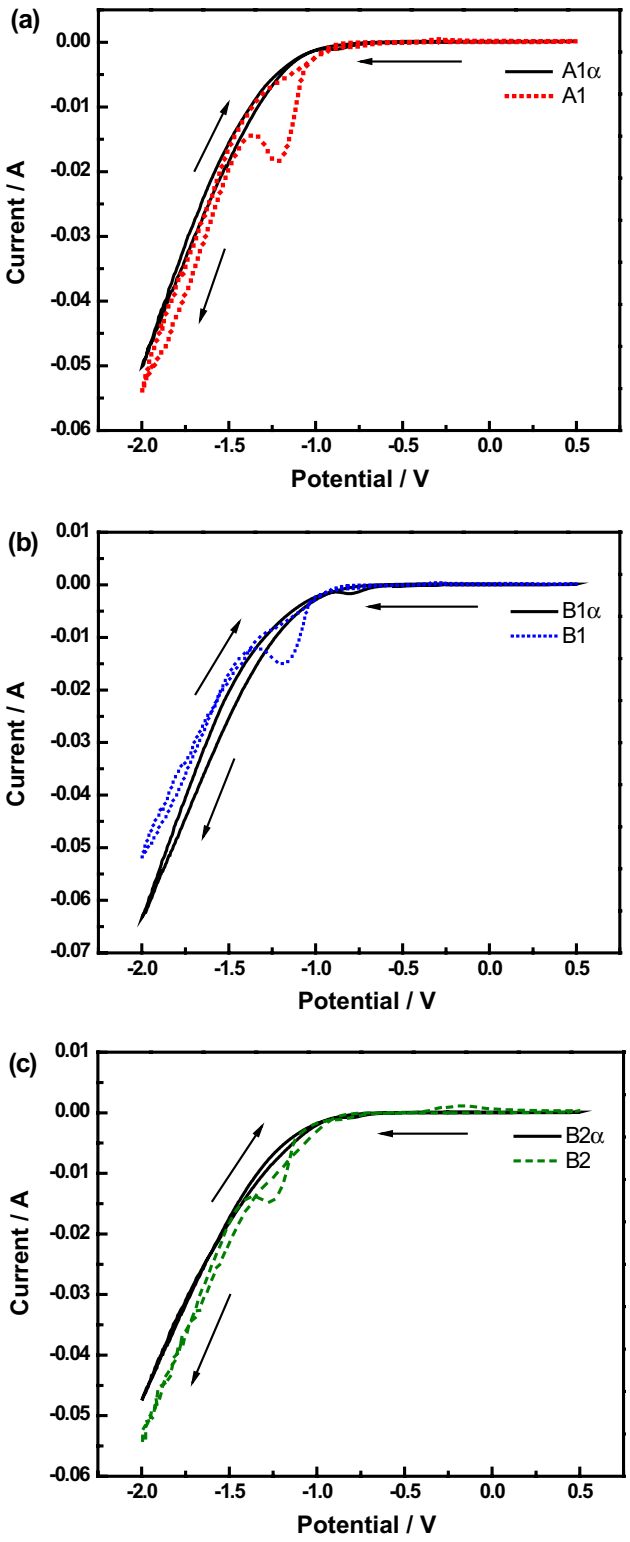

Fig. 1 Cyclic voltammetry study of all bath solutions at a scan rate of 10 mV s^{-1}; **a** sample without nickel (A1α) and with nickel (A1), **b** sample without nickel (B1α) and with nickel (B1), **c** sample without nickel (B2α) and with nickel (B2)

The small anodic peak on the reverse scan at ~−0.30 V is due to the nickel metal oxidizing to nickel oxide on the surface. Anodic peak current, $i_{pa,}$ in all solutions is minimal, and the organic modifier appears to have little effect on the anodic potential, E_{pa}, and i_{pa}.

3.2 Deposition conditions for Ni coatings

A modified pulse deposition provides more uniform coatings of nickel, and the upper and lower potentials were chosen after analyzing the CV studies [12]. The results of the CV study led to the selection of an upper deposition potential of −1.08 V, to minimize hydrogen evolution at the electrode surface but still provide a large enough overpotential to deposit nickel from solution. Deposition of A1 (no organic modifier) was used as a benchmark to test deposition quality for cathodic potentials between −1.0 V and −1.2 V; −1.08 V produced good quality and uniform nickel coatings with minimal hydrogen evolution. The lower potential of −0.6 V was determined experimentally and selected as the potential where approximate zero current flow was observed. A running scan rate of 100 mV s^{-1} between these potentials was selected because it produced more uniform deposits versus a square wave potential step method [45]. The deposition waveform was cycled until ~40 C of charge was obtained to provide full coverage of the substrate. Thickness of the coatings was measured using a profilometer and averaged 6.30 ± 0.11 µm for this amount of charge. Coating thicknesses did not vary with addition of butanol to the solution. Even though conductivity of the plating solution was slightly lowered with the organic addition, it was still high enough to allow good plating of the nickel; A1 = 26.53 ± 0.57, B1 = 23.01 ± 0.64, and B2 = 21.46 ± 0.57 mS cm^{-1}. The appearance of all coatings was similar (Supplemental Fig. 1) and semi-bright in appearance.

3.3 X-ray diffraction (XRD) of Ni coatings

The effects of the addition of BuOH on the crystal orientation of nickel were investigated with powder XRD, and results are presented in Fig. 2. Two predominant peaks are observed for each nickel coating, the (111) and (220) reflections. These peaks are characteristic for face-centered cubic (fcc) nickel, although the XRD patterns showed preferred orientation (220) for the coatings. This mixed phase is a result of a lower reduction potential of −1.08 V applied during deposition of the coatings. Both Abel and Cortes reported that a lower overpotential can cause a preference for (110) growth planes when current density is low, or in the presence of wetting or brightening agents [46, 47]. Samples B1 and B2, containing butanol, also display (220) preferred growth but slightly more (111) character, again

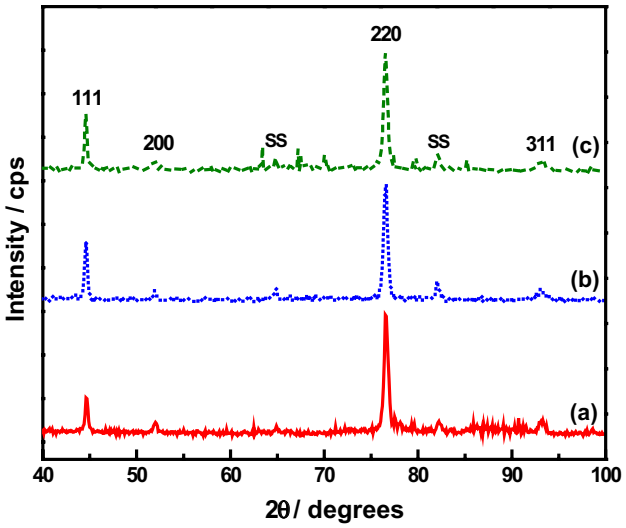

Fig. 2 X-ray diffraction patterns of each nickel coating *a* A1 (*solid line*), *b* B1 (*dotted line*), and *c* B2 (*dashed line*)

Table 2 Relative texture coefficients for (111), (200), (220), and (311) growth planes for each sample as measured with XRD

Sample	RTC_{111}	RTC_{200}	RTC_{220}	RTC_{311}
A1	5.26	4.85	72.32	17.66
B1	8.09	4.32	71.84	15.74
B2	7.80	4.27	72.66	15.26

consistent with the observed cathodic reduction potential shift of nickel. To better understand the influence of how organic addition influences preferred orientation of the coatings, relative peak intensities were analyzed by determining relative texture coefficients of the peaks [(111), (200), (220), and (311)] present in the XRD patterns. Additionally, due to the polycrystalline nature of the coatings, determining which orientation is more beneficial for corrosion resistance was of interest as well. The relative texture coefficient (RTC_{hkl}) for each orientation was calculated as shown in Eq. [1] and is related to the corrosion resistance of the films.

$$RTC_{hkl} = \frac{I_{p,hkl}/I^{\circ}_{p,hkl}}{\sum I_{p,hkl}/I^{\circ}_{p,hkl}} \times 100\% \quad (1)$$

where $I_{p,hkl}$ is the intensity of the peak for each sample at (111), (200), (220), and (311) reflections and $I^{\circ}_{p,hkl}$ is the intensity of those reflections for the nickel standard reference (PDF# 00-004-0850) [18, 48]. The standard provides a random orientation pattern to compare against any preferred orientation found in the samples. Results are listed in Table 2. Sample A1 has a relative texture coefficient of 72.32 for the predominant (220) reflection, 5.26 for (111),

4.85 for (200), and 17.66 for (311). Samples B1 and B2 display RTC values for (220) similar to that of A1, at 71.84 and 72.66, respectively, also consistent with the cathodic shift in nickel reduction potential. The noticeable increase in (111) and decrease in (311) coefficients for B1 and B2 suggest that the addition of butanol inhibits the (220) orientation in favor of a (111) orientation.

Organic addition into the plating bath was previously shown to lead to coating microcracking and internal strain in nickel electrodeposits [34]. Since relative texture coefficient analysis showed that BuOH addition does affect the growth mechanism of the nickel coating, Williamson–Hall analysis was performed to determine if any strain could be observed for the coatings from BuOH addition. A correction for instrumental broadening was done using a Si powder 325 mesh (Alpha Aesar) sample which matched the PDF# 00-027-1402 file. The particle size and strain were calculated by obtaining the full width at half maximum (FWHM) of the nickel peaks for reflections (111), (220), and (311) using Eq. [2],

$$B_r^2 = B_0^2 - B_i^2 \quad (2)$$

where B_r equals the corrected FWHM of each peak, B_o is the observed FWHM of the nickel film peaks, and B_i is the instrumental broadening value calculated from a 325 mesh silicon powder standard pattern. Lattice strain and particle size (Table 3) were determined by plotting $B_r\cos\theta$ versus $\sin\theta$ (Supplemental Fig. 2) for the corrected nickel peaks. The minimal strain for each coating most likely is due to the presence of boric acid and the absence of allylic groups on the organic modifier [41]. The low strain values are promising results for these nickel coatings that are deposited using the aqueous/organic baths. Particle size was in the nanometer range from ~16 to 35 nm, which would be expected for films deposited from a borate electrolyte and organic modifier solution by a pulse deposition [10–12, 26, 27].

3.4 Surface morphology

All samples were examined with scanning electron microscopy (SEM) after electrodeposition (Fig. 3). For the freshly deposited samples, a uniform coating across the surface was observed with smooth fine-grained deposit and no microcracking present. These results fit well with strain results from Williamson–Hall analysis, showing minimal strain for coatings deposited with high concentrations of butanol; unlike DMF, where microcracking is observed at higher concentrations [28]. All samples were nanocrystalline, as determined with XRD, and similar in morphology. The presence of (220) geometry appears as pyramidal structures, but due to the mixed (111) and (220) orientations, the surface comprises a hybrid geometrical appearance for all the samples [27]. Samples B1 and B2 appear to have smaller grains than that of A1.

Table 3 Strain and particle size of each sample as determined from Williamson–Hall analysis of the X-ray diffraction data

Sample	Strain (η)	Particle size (nm)
A1	0.0083	16.09
B1	0.0043	19.05
B2	0.0175	34.48

3.5 Corrosion studies

3.5.1 Open circuit potential (OCP) immersion studies

After electrodeposition, the coatings were submerged in a 3.5% NaCl solution to simulate corrosion, and OCP was monitored for 14 days prior to Tafel polarization and EIS analysis. A time period of 14 days was chosen, since experiments showed that this was the time needed to form a full oxide layer allowing complete passivation for the nickel coatings. Measurements taken at the end of this time period determined the degree of breakdown or permeability of chloride ions for this passive oxide. Immersion study results are presented in Fig. 4. All samples showed anodic shifts in OCP, due to the formation of an oxide layer that provides barrier protection, and evidence of generalized corrosion on the surface for all samples (Supplemental Fig. 3). Sample B2 maintained the most anodic OCP at −0.252 V. After 14 days, each sample was analyzed by linear polarization to determine E_{corr} and i_{corr} values. Each sample was immersed in fresh NaCl (3.5%) for 1 h, until a stable OCP was reached prior to analysis.

3.5.2 Electrochemical impedance spectroscopy

Electrochemical impedance (EIS) was run to better understand how BuOH addition affects corrosion resistance of the electrodeposited nickel coatings after a 14-day soak. ZView software was used to model EIS results and calculate equivalent circuit values of each circuit element. Each sample was normalized to a 1.0 cm^2 area and was modeled successfully. The equivalent circuit model shown in the inset of Fig. 5 contains five elements, three resistors, and three constant phase elements, which model non-ideal capacitors. The circuit models a nickel coating layer with a thin passive oxide layer that displays some micropores within the coating. The oxide layer will have formed after the immersion time, but would be thin compared to the nickel coating. For this circuit, R_s represents resistance of the 3.5% NaCl solution, CPE_f represents capacitance of the passive coating where α_1 is a

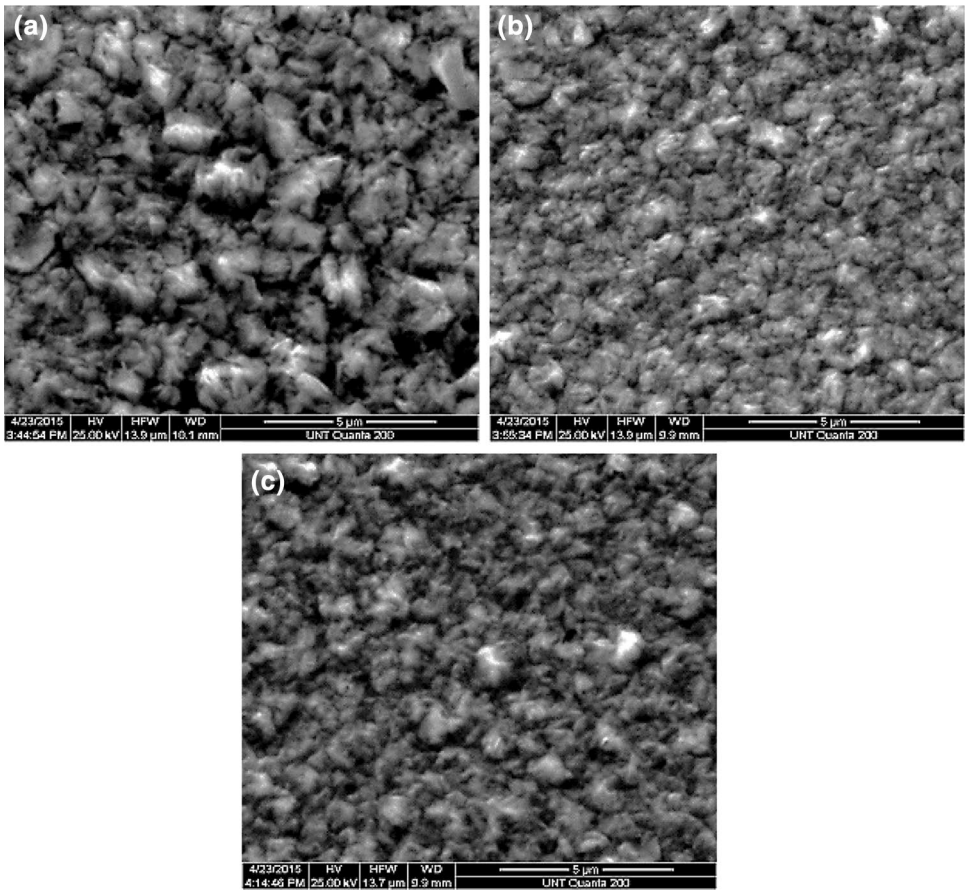

Fig. 3 SEM images of each nickel coating **a** A1, **b** B1, and **c** B2. (magnification −×25,000)

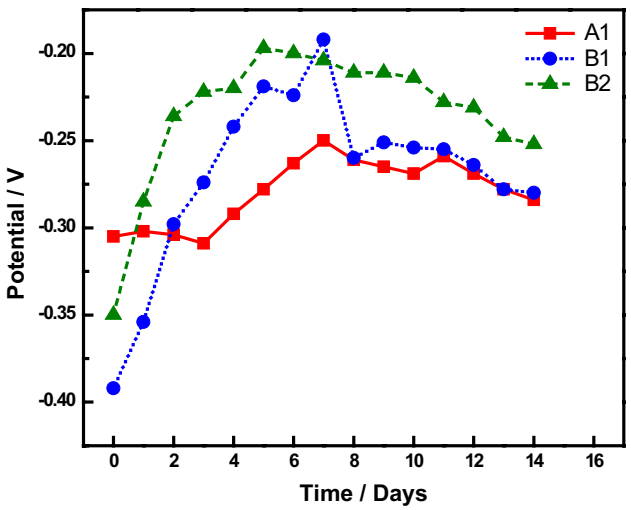

Fig. 4 OCP versus time for each nickel coating immersed in 3.5% NaCl solution for 14 days. (A1 *squares* + *solid line*, B1 *circles* + *dotted line*, B2 *triangles* + dashed *lines*)

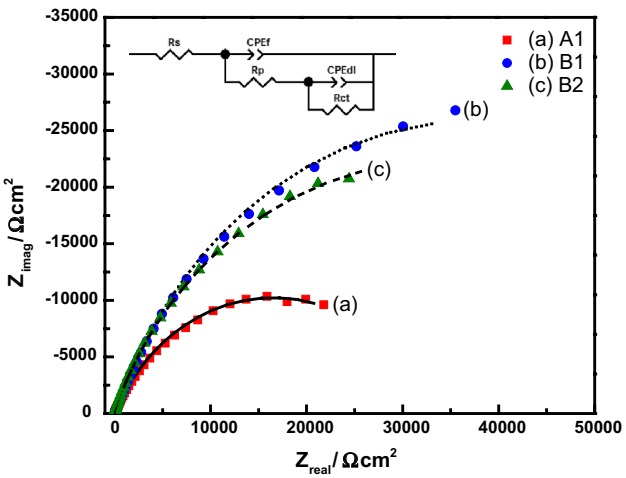

Fig. 5 Nyquist plots and fittings for nickel coatings *a* A1, *b* B1, and *c* B2, using the circuit displayed in the *inset*. *Lines* are the fitting *curves* and the *symbols* represent the data from the EIS experiment

coefficient between 0 and 1, where 1 signifies an ideal capacitor. R_p portrays the resistance of the electrochemical reaction between the solution and the nickel coating, both on the surface and within the micropores [49]. CPE_{dl} and α_2 describe the double layer capacitance between the electrolyte and the coating interface at the bottom of the pores. R_{ct} is the charge transfer resistance, which

is related to corrosion resistance. This circuit model matches what other researchers have measured for nickel coatings on steels [49–51]. The calculated values for the circuit elements are listed in Table 4.

The Nyquist and Bode plots for EIS are shown in Figs. 5 and 6, respectively. Nyquist plots and fittings for each sample show a distinct single semicircle pattern (Fig. 5). Values for R_s range between 10 and 13 Ω and display a reliable fit for each sample (Table 4). The slight increase of R_p for B1 and B2 over A1 indicates an increase in passive film resistance. B1 and B2 display larger capacitive loop diameters, giving larger R_{ct} values compared to A1, and a higher resistance to corrosion. This increase is most likely due to the smaller grain sizes of the deposits. Smaller grain sizes effectively increase the total surface area of the deposits, resulting in a faster rate of oxidation needed for passivation. Sample B1 exhibits the highest R_{ct} value at 73,672 Ω cm^2, nearly double the value for A1. Increasing the percentage of BuOH to 10%, in B2, leads to a slight drop in $R_{ct,}$ but only negligible decreases in R_p. When butanol is present during deposition, it modifies the deposition of nickel, possibly by stabilizing the NiOH colloid, slowing the rate of deposition and decreasing the grain size of the deposited nickel. Thus, corrosion is slower, and the passive layer forms more quickly for these films.

Bode phase angle plots were studied to determine how phase angle values model capacitive effects and corrosion-resistant behavior of the coatings. All coatings tested displayed a broad phase angle maximum, characteristic of the two time constants, which is consistent with the circuit model and fitting. This suggests two capacitive responses, first for the interface between the nickel coating and the substrate, and the other due to a concentration gradient of NaCl ions that have diffused through micropores into the passive oxide layer. This is displayed as a second maxima in the lower frequency regions for all samples [52]. All coatings approach 0° in the high frequency region, and the phase angle maximum occurred between 30 and 50 Hz for every coating except for sample B1, which occurred at 2 Hz. In the lower frequency range, sample A1 shows the lowest value, followed by B2 and B1. B1 sustains a higher phase angle value through the lower regions, which denotes the most capacitive behavior and is indicative of a smaller particle size and surface charge. B1 and B2 phase angles closer to 90° than A1 connote a more stable passive film.

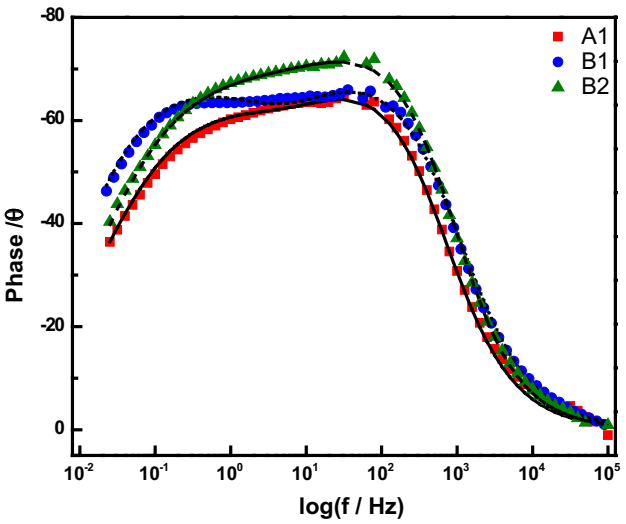

Fig. 6 *Bode phase angle* plots for nickel coating samples. *Lines* are the fitting *curves* and the *symbols* represent the data from the EIS experiment

3.5.3 *Potentiodynamic polarization measurements*

Potentiodynamic polarization scans from −0.25 to 1.0 V were run on fresh coatings, to measure their resistance to corrosion in the active region of the scan, where the dominant reaction is oxidation of nickel. (See supplemental section Fig. 4; Table 1). The passive region formed for the fresh coatings is minimal compared to the soaked coatings, but allows a measure of how thick a passive layer can be formed for the different coatings. Fresh coatings deposited from the solutions containing BuOH have rest potentials (E_{corr}) cathodic to A1, and a higher β_a slope, which indicates an ability to form an oxide layer more readily. The breakdown potential (E_{bd}) is located after the passive region, where the large onset of current points to failure of the coating due to pitting or crevice corrosion reaching the steel substrate. By measuring the difference between rest potential and breakdown potential, resistance of the passive layer to breakdown can be measured for each coating. Samples B1 and B2 displayed the largest difference in the active region (100 and 50 mV wider than A1, respectively), and show that smaller grain size promotes quicker onset of oxide layer formation. Addition of BuOH in

Table 4 Calculated circuit elements generated using ZView software from the EIS data

Sample	R_s (Ω)	CPE$_f$ (μF cm^{-2})	α_1	R_p (Ω cm^2)	CPE$_{dl}$ (μF cm^{-2})	α_2	R_{ct} (Ω cm^2)
A1	12.99	75.3	0.826	945	81.6	0.625	32,653
B1	10.13	73.2	0.813	1662	50.8	0.718	73,672
B2	10.58	49.3	0.869	1656	38.3	0.610	69,290

Table 5 E_{corr} and i_{corr} corrosion values for the nickel coatings calculated from linear polarization measurements

Sample	E_{corr} (V)	i_{corr} (A cm^{-2})	β_a (V dec^{-1})	β_c (V dec^{-1})
A1	−0.405	1.99×10^{-7}	0.185	0.393
B1	−0.234	3.35×10^{-7}	0.190	0.195
B2	−0.343	2.14×10^{-7}	0.241	0.191

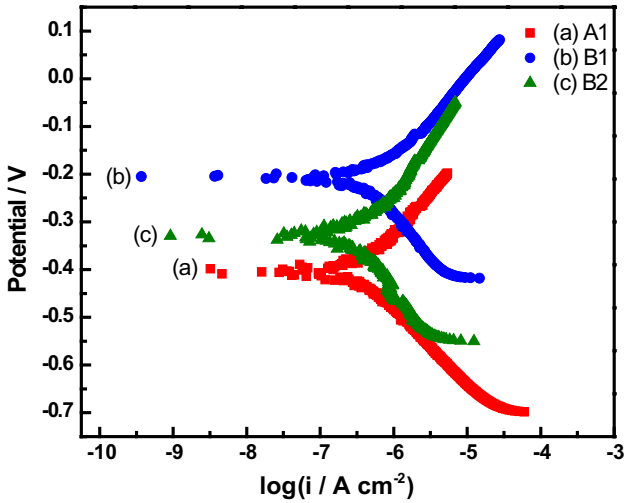

Fig. 7 Tafel polarization curves for each coating *a* A1 (*squares*), *b* B1 (*circles*), and *c* B2 (*triangles*) run in 3.5% NaCl after 14 days immersion in 3.5% NaCl

the plating bath improves initial oxide layer formation for the nickel coating, and fits the EIS results.

Linear polarization was carried out for the coatings after soaking for 14 days in a 3.5% NaCl solution. Coatings were immersed in a fresh 3.5% NaCl solution and scanned ±250 mV from OCP in both directions. E_{corr} and estimated i_{corr} values were measured by locating the intersection point of the extrapolated linear sections of the anodic (β_a) and cathodic (β_c) portions of the scan. The results are listed in Table 5 and Fig. 7 for each coating. Sample sets containing the organic modifier display better passivation than sample A1, which can be seen from the slope of β_a and the E_{corr} values for B1 and B2. The slope of this linear region represents a passivity due to a thicker oxide layer. The i_{corr} values were all in the same range of 10^{-7} A cm^{-2}, with A1 displaying the lowest estimated corrosion current. The value of i_{corr} as affected by the angle of the cathodic and anodic slopes suggests that a larger anodic slope (β_a) will intersect with the E_{corr} line at a higher value of log(i). The anodic slope, $\beta_{a,}$ describes the onset of passivation and the rate at which a passive oxide layer forms. Corrosion studies again show improved corrosion resistance when more BuOH is added to the plating bath.

4 Conclusions

- Smooth and uniform semi-bright nickel coatings were successfully synthesized from a low nickel concentration all-sulfate bath containing larger amounts of organic modifier, 5 and 10% butanol.
- Nickel coatings displayed minimal strain and nanocrystalline particle size using a pulse potential deposition at room temperature.
- The presence of BuOH cathodically shifted hydrogen evolution for the deposition, which affected the preferred orientation of the films, and the grain size of the nickel deposits.
- After 14 days' immersion in 3.5% NaCl, B1 and B2 resistance to corrosion was improved with a twofold increase in the R_{ct} value (73,672 Ω cm^2) over A1.
- Linear polarization displayed an anodic shift of E_{corr} for both B1 and B2, due to the development of a thicker passive oxide layer.

Acknowledgements The authors thank Casey Thurber and Stephen Sanders for obtaining SEM data and Dr. Heidi Conrad for helpful scientific discussions. The authors also acknowledge the Center for Advanced Research and Technology (CART) and AMMPI (Advanced Materials and Manufacturing Processes Institute) at the University of North Texas.

References

1. Hihara LH (2015) Electrochemical aspects of corrosion-control coatings, Elsevier Inc., Amsterdam
2. Selvaraj R, Selvaraj M, Iyer SVK (2009) Studies on the evaluation of the performance of organic coatings used for the prevention of corrosion of steel rebars in concrete structures. Prog Org Coat 64(4):454–459
3. Elias L, Hegde CA (2015) Electrodeposition of laminar coatings of Ni–W Alloy and their corrosion behaviour. Surf Coat Technol 283:61–69
4. Thurber CR, Ahmad YH, Sanders SF, Al-Shenawa A, D'Souza N, Mohamed AMA, Golden TD (2016) Electrodeposition of 70–30 Cu–Ni nanocomposite coatings for enhanced mechanical and corrosion properties. Curr Appl Phys 16:387–396
5. Coskun MI, Karahan IH, Yucel Y, Golden TD (2016) Computer-assisted optimization of electrodeposited hydroxyapatite coating parameters on medical alloys. Metall Mater Trans A, 47(4):1828–1841
6. Parkinson R. (1997) Properties and applications of electroless nickel. Nickel Development Institute, Toronto, pp 1–33
7. Di Bari GA (2010) Electrodeposition of Nickel. In: Schlesinger M, Paunovic M (eds), Modern electroplating 5th edn. John Wiley & Sons, Inc., Hoboken, pp 79–114
8. Dennis JK, Such TE (1986) Nickel and Chromium Plating, 2nd edn. Butterworth and Co LTD, Cambridge, p 151
9. Lee RT, Liu CT, Chiou YC, Chen HL (2013) Effect of nickel coating on the shear strength of fsw lap joint between Ni–Cu alloy and steel. J Mater Process Tech 213(1): 69–74

10. Kumar KS, Suresh S, Chisholm MF, Horton JA, Wang P (2003) Deformation of electrodeposited nanocrystalline nickel. Acta Mater 51(2):387–405
11. Meng G, Sun F, Shaoa Y, Zhang T, Wang F, Dong C, Li X (2010) Effect of phytic acid on the microstructure and corrosion resistance of Ni coating. Electrochim Acta 55(20):5990–5995
12. Tang PT, Watanabe T, Andersen, JET, Bech-Nielsen G (1995) Improved corrosion resistance of pulse plated nickel through crystallisation control. J Appl Electrochem 25:347–352
13. Peng X, Zhang Y, Zhao J, Wang F (2006) Electrochemical corrosion performance in 3.5% NaCl of the electrodeposited nanocrystalline Ni Films with and without dispersions of Cr nanoparticles. Electrochim Acta 51:4922–4927
14. Walsh FC, Ponce de Leon C (2014) A review of the electrodeposition of metal matrix composite coatings by inclusion of particles in a metal layer: an established and diversifying technology. Trans Inst Met Finish 92(2):83–98
15. Simunkova H, Pessenda-Garcia P, Wosik J, Angerer P, Kronberger H, Nauer GE (2009) The fundamentals of nano- and submicro-scaled ceramic particles incorporation into electrodeposited nickel layers: zeta potential measurements. Surf Coat Technol 203(13):1806–1814
16. Khoramkhorshid S, Alizadeh M, Taghvaei AH, Scudino S (2016) Microstructure and mechanical properties of Al-based metal matrix composites reinforced with $Al_{84}Gd_6Ni_7Co_3$ glassy particles produced by accumulative roll bonding. Mater Des 90:137–144
17. Shibli SMA, Chacko F (2008) Development of nano CeO_2-incorporated high performance hot-dip zinc coating. Surf Coat Technol 202(20):4971–4975
18. Ahmad YH, Tientong J, D'Souza N, Golden TD, Mohamed AMA (2014) Surface & coatings technology salt water corrosion resistance of electrodeposited Ni-layered silicate nanocomposite coatings from Watts' type solution. Surf Coat Technol 242:170–176
19. Addi Y, Duverneuil P, Khouider A (2011) Zinc nickel codeposition in ammonium sulfate combined effect of cadmium and boric acid. ECS Trans 33(26):75–82
20. Hoare JP (1987) Boric acid as a catalyst in nickel plating solutions. J Electrochem Soc 134(12):3102–3103
21. Karwas C, Hepel T (1987) Influence of boric acid on electrodeposition and stripping of Ni-Zn alloys. J Electrochem Soc 135(4):839–844
22. Supicova M, Rozik R, Trnkova L, Orinakova R, Galova M (2006) Influence of boric acid on the electrochemical deposition of Ni. J Solid State Electrochem 10: 61–68
23. Addi Y, Khouider A (2013) Electrodeposition of Ni–Zn alloys on steel from acidic solution in presence of boric acid. ECS Trans 45(24):79–85
24. Ji J, Cooper C, Dreisinger DB, Peters E (1995) Surface pH measurements during nickel electrodeposition. J Appl Electrochem 25: 642–650
25. Dávalos CE, López JR, Ruiz H, Méndez A, López RA, Trejo G (2013) Study of the role of boric acid during the electrochemical deposition of Ni in a sulfamate bath. Int J Electrochem Sci 8:9785–9800
26. Conrad HA, McGuire MR, Zhou T, Coskun MI, Golden TD (2015) Improved corrosion resistant properties of electrochemically deposited zinc-nickel alloys utilizing a borate electrolytic alkaline solution. Surf Coat Technol 272:50–57
27. Costavaras T, Froment M, Hugot-Le Goff A, Georgoulis C (1973) The influence of unsaturated organic molecules in the electrocrystallization of nickel. J Electrochem Soc 4: 867–874
28. Srivastava HK, Tikoo PK (1987) Electrodeposition of nickel from *N, N*-dimethylformamide. Surf Coatings Technol 31(4):343–350
29. Bakhit B, Akbari A (2014) A comparative study of the effects of saccharin and b-SiC nano-particles on the properties of Ni and Ni–Co alloy coatings. Surf Coat Technol 253: 76–82
30. Wu W, Eliaz N, Gileadi E (2016) Electrodeposition of Re–Ni alloys from aqueous solutions with organic additives. Thin Solid Films 616: 828–837
31. Mirzamohammadi S, Khorsand H, Aliofkhazraei M (2017) Effect of different organic solvents on electrodeposition and wear behavior of Ni–Alumina nanocomposite coatings. Surf Coat Technol 313: 202–213
32. Seleim SM, Ahmed AM, El Adl AF (2014) Electroplating in steel in presence of isopropanol-water mixture. Int J Electrochem Sci 9(4):2016–2028
33. Rao NN, Singh VB (1985) Behavior of copper formamide-water mixtures. Corros Sci 25(7):471–482
34. Sultan S, Tikoo PK (1984) Hardness and structure of nickel electrodeposited from a nickel acetate-*N, N*-dimethylformamide-water bath. Surf Technol 21(3):239–244
35. Tripathi MK, Singh DK, Singh VB (2013) Electrodeposition of Ni-Fe/Bn nano-composite coatings from a non-aqueous bath and their characterization. Int J Electrochem Sci, 8(3):3454–3471
36. An MZ, Wang JL, Sun DZ (2001) Electrodeposition of La–Ni alloy films in a nonaqueous system. J Appl Electrochem 31: 891–896
37. Macheras J, Vouros D, Kollia C, Spyrellis N (1996) Nickel electrocrystallization: influence of unsaturated organic additives on the mechanism of oriented crystal growth. Trans Inst Met Finish 74(2):55–58
38. Nakamura Y, Kaneko N, Watanabe M, Nezu H (1994) Effects of saccharin and aliphatic alcohols on the electrocrystallization of nickel. J Appl Electrochem 24: 227–232
39. Belkis U, Esma S, Ramazan K (2013) The investigation of electrochemical effect of diol compounds in nickel electroplating bath. J Mater Sci Eng Adv Technol 8(2):55–68
40. Niederberger M, Garnweitner G, Buha J, Polleux J, Ba J, Pinna N (2006) Nonaqueous synthesis of metal oxide nanoparticles: review and indium oxide as case study for the dependence of particle morphology on precursors and solvents. J Sol-Gel Sci Technol 40:259–266
41. Graham LM, Cho S, Kim SK, Noked M, Lee SB (2014) Role of boric acid in nickel nanotube electrodeposition: a surface-directed growth mechanism. Chem Commun 50: 527–529
42. Henderson WG, How MJ, Kennedy GR, Mooney EF (1973) The interconversion of aqueous boron species and the interaction of borate with diols: A ^{11}B N.M.R. study. Carbohydr Res 28: 1–12
43. Zhitomirsky I (2002) Cathodic electrodeposition of ceramic and organoceramic materials. Fundam Asp 97:279–317
44. De Hazan Y, Knies F, Burnat D, Graule T, Yamada-Pittini Y, Aneziris C, Kraak M (2012) Homogeneous functional Ni–P/Ceramic nanocomposite coatings via stable dispersions in electroless nickel electrolytes. J Colloid Interface Sci 365:163–171
45. Conrad H, Corbett J, Golden TD (2012) Electrochemical deposition of g-Phase zinc-nickel alloys from alkaline solution. J Electrochem Soc 159(1):C29–C32
46. Abel S, Freimuth H, Lehr H, Mensinger H (1999) Defined crystal orientation of nickel by controlled microelectroplating. J Micromech Microeng 4:47–54
47. Cortes A, Riveros G, Palma JL, Denardin JC, Marotti RE, Dalchiele EA, Gomez H (2009) Single-crystal growth of nickel nanowires: influence of deposition conditions on structural and magnetic properties. J Nanosci Nanotechnol 9(3):1992–2000
48. Rashidi AM, Hayati M, Rezaei A (2011) Prediction of the relative texture coefficient of nanocrystalline nickel coatings using artificial neural networks. Solid State Sci 13(8):1589–1593
49. Magana-Zavala CR, Angeles-San Martin ME, Rodriguez-Gomez FJ, Acosta DR, Avila-Godoy R, Hidalgo-Prada B (2010)

Electrochemical impedance spectroscopy (EIS) modelling of different behaviours of Ni and Ni oxide thin films for corrosion prevention in sour media. Anti-Corros Methods Mater 57(3):118–125

50. Hashemzadeh M, Raeissi K, Khorsund AS (2015) Effect of ammonia chloride on microstructures, super-hydrophobicity and corrosion resistance of nickel coatings. Surf Coat Technol 283:318–328
51. Meng G, Li Y, Shao Y, Zhang T, Wang Y, Wang F, Cheng X, Dong C, Li X (2015) Effect of microstructures on corrosion behavior of nickel coatings: (i) abnormal grain size effect on corrosion behavior. J Mater Sci Technol 31:1186–1192
52. Drevet R, Aaboubi O, Benhayoune H (2012) In vitro corrosion behavior of electrodeposited calcium phosphate coatings on Ti6Al4V Substrates. J Solid State Electrochem 16(9): 3069–3077